ACS chemical biology

Articles

Cite This: ACS Chem. Biol. XXXX, XXX, XXX−XXX

pubs.acs.org/acschemicalbiology

Molecular Basis of *Bacillus subtilis* ATCC 6633 Self-Resistance to the Phosphono-oligopeptide Antibiotic Rhizocticin

Nektaria Petronikolou,[†,⊥] Manuel A. Ortega,[‡,⊥] Svetlana A. Borisova,[‡] Satish K. Nair,[*,†,‡,§] and William W. Metcalf[*,‡,∥]

[†]Department of Biochemistry, University of Illinois at Urbana−Champaign, Roger Adams Laboratory, 600 S. Mathews Ave., Urbana, Illinois 61801, United States

[‡]Carl R. Woese Institute for Genomic Biology, University of Illinois at Urbana−Champaign, 1206 W. Gregory Drive, Urbana, Illinois 61801, United States

[§]Center for Biophysics and Computational Biology, University of Illinois at Urbana−Champaign, Roger Adams Laboratory, 600 S. Mathews Ave., Urbana Illinois 61801, United States

[∥]Department of Microbiology, University of Illinois at Urbana−Champaign, Chemical and Life Sciences Laboratory, 601 S. Goodwin Ave., Urbana, Illinois 61801, United States

Supporting Information

ABSTRACT: Rhizocticins are phosphono-oligopeptide antibiotics that contain a toxic C-terminal (*Z*)-L-2-amino-5-phosphono-3-pentenoic acid (APPA) moiety. APPA is an irreversible inhibitor of threonine synthase (ThrC), a pyridoxal 5′-phosphate (PLP)-dependent enzyme that catalyzes the conversion of *O*-phospho-L-homoserine to L-threonine. ThrCs are essential for the viability of bacteria, plants, and fungi and are a target for antibiotic development, as *de novo* threonine biosynthetic pathway is not found in humans. Given the ability of APPA to interfere in threonine metabolism, it is unclear how the producing strain *B. subtilis* ATCC 6633 circumvents APPA toxicity. Notably, in addition to the housekeeping APPA-sensitive ThrC (*Bs*ThrC), *B. subtilis* encodes a second threonine synthase (RhiB) encoded within the rhizocticin biosynthetic gene cluster. Kinetic and spectroscopic analyses show that PLP-dependent RhiB is an authentic threonine synthase, converting *O*-phospho-L-homoserine to threonine with a catalytic efficiency comparable to *Bs*ThrC. To understand the structural basis of inhibition, we determined the crystal structure of APPA bound to the housekeeping *Bs*ThrC, revealing a covalent complex between the inhibitor and PLP. Structure-based sequence analyses reveal structural determinants within the RhiB active site that contribute to rendering this ThrC homologue resistant to APPA. Together, this work establishes the self-resistance mechanism utilized by *B. subtilis* ATCC 6633 against APPA exemplifying one of many ways by which bacteria can overcome phosphonate toxicity.

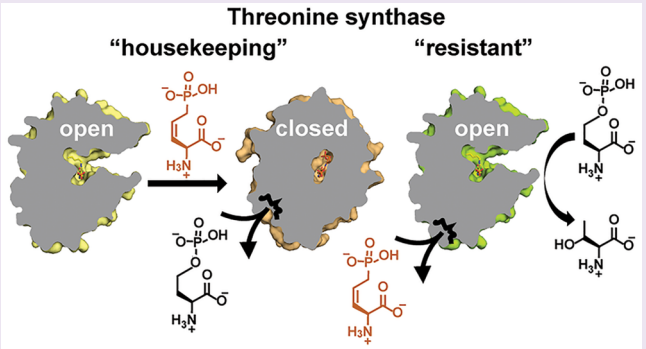

Phosphonates are natural products characterized by the presence of an inert C−P bond in place of the more common O−P bond found in phosphoric acids.[1] As structural analogs of numerous phosphate ester and carboxylic acid intermediates found in metabolic processes, phosphonates act as inhibitors of the corresponding enzymes. For instance, the unusual nonproteinogenic amino acid (*Z*)-L-2-amino-5-phosphono-3-pentenoic acid (APPA) inhibits threonine synthases (ThrC) irreversibly by mimicking the physiological substrate *O*-phospho-L-homoserine (PHSer) (Figure 1a).[2,3] ThrC is a pyridoxal 5′-phosphate (PLP)-dependent enzyme that utilizes PHSer as a substrate in the last step in threonine biosynthesis (Figure 1a).[4,5]

APPA is the pharmacophore present at the C-terminus of the phosphono-oligopeptide antifungal rhizocticin,[6] produced by the Gram-positive bacterium *Bacillus subtilis* ATCC 6633 (Figure 1b).[7] Notably, APPA is also found as the active warhead of plumbemycins, which are antibacterial tripeptides produced by *Streptomyces plumbeus*.[8,9] Although both phosphono-oligopeptides contain a C-terminal APPA residue, they contain different amino acids at their N-terminus. This difference is believed to be responsible for defining the spectrum of target organisms affected by the two natural products. Thus, due to differences in the specificities of oligopeptide transporters, rhizocticin has antifungal but not antibacterial activity, while plumbemycin has the opposite spectrum. In either case, host peptidases cleave the peptide to

Received: January 9, 2019
Accepted: March 4, 2019
Published: March 4, 2019

DOI: 10.1021/acschembio.9b00030
ACS Chem. Biol. XXXX, XXX, XXX−XXX

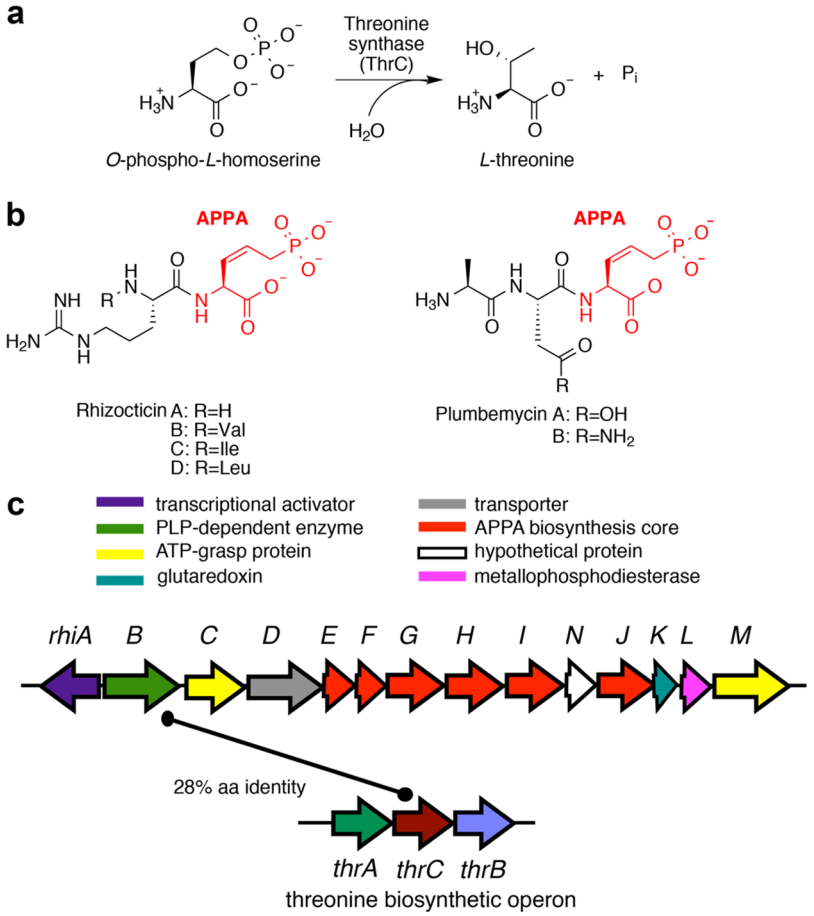

Figure 1. Overview of rhizocticin biosynthetic gene cluster. (a) Reaction catalyzed by threonine synthases (*Bs*ThrC), which is inhibited by APPA. (b) Structure of the phosphono-oligopeptides rhizocticin and plumbemycin. The nonproteinogenic phosphono-amino acid (*Z*)-L-2-amino-5-phosphono-3-pentenoic acid is shown in red. (c) Rhizocticin biosynthetic gene cluster. Biosynthetic genes are shown in red and the putative gene involved in self-resistance, RhiB, is shown in green. For comparison, the *B. subtilis* ATCC 6633 threonine biosynthetic operon is shown below indicating the percent amino acid sequence identity between the predicted threonine synthase homologue RhiB and the *Bs*ThrC.

release the C-terminal APPA warhead after uptake, resulting in growth inhibition.[10]

Early *in vivo* antagonist experiments with various amino acids suggested that APPA caused growth inhibition by disrupting threonine-related metabolism.[8,10] *In vitro* experiments later revealed APPA to be an irreversible inhibitor of the threonine biosynthetic enzyme ThrC, demonstrating saturation kinetics with an apparent k_{inact} of 1.50 min^{-1} and a K_i of 100 μM.[2,3] Plausible mechanisms for inhibition include covalent modification of the enzyme or modification of the PLP cofactor, but the experimental data did not provide support for either of these proposed mechanisms.[2] In these studies, APPA inhibited the threonine synthase from *E. coli* (*Ec*ThrC) irreversibly at a molar ratio of 1:1 suggesting that inhibition occurs through formation of a covalent adduct between APPA and the enzyme.[2,3] This mode of inhibition is observed in other PLP-dependent enzymes such as inhibition of 1-aminocyclopropane-1-carboxylate synthase by L-vinylglycine.[11] However, tryptic digestion of *Ec*ThrC and peptide analysis did not reveal any modified peptides.[2] This finding led the authors to propose a mechanism of inhibition that involves a conformational change of the enzyme leading to the stabilization of an enzyme−inhibitor complex, a mechanism similar to the one of D-amino acid aminotransferase inhibition by the antibiotic D-cycloserine.[2,12,13] Thus, despite almost 14 years since the identification of APPA as an inhibitor of ThrC, the molecular details regarding the mechanism of inactivation remain unclear.

ThrC is an essential enzyme for growth of bacteria and fungi, and this enzyme is not present in mammals. Given the widespread occurrence of antibiotic resistance and the impending need for the identification of novel antibiotics, ThrC is a worthwhile microbial target, and APPA is an attractive therapeutic candidate.[14] As such, understanding the mechanism of inhibition of ThrC by APPA as well as how the producing organisms overcome APPA toxicity will inform on the clinical potential of APPA.

Previous bioinformatic studies on the rhizocticin biosynthetic gene cluster identified the *rhiB* gene, whose product showed homology to threonine synthases (Figure 1c).[15] Curiously, examination of the *B. subtilis* ATCC 6633 genome also reveals the presence of a threonine biosynthetic operon (*thrACB*), which is similar in genomic context and sequence to the typical *Bacillus* threonine synthase involved in primary metabolism (*Bs*ThrC) (Figure 1c).[5,15,16] Sequence alignment between RhiB and *Bs*ThrC revealed that they share greater than 25% sequence identity further suggesting that RhiB is a threonine synthase (Figure 1c). These observations prompted us to consider that RhiB could function as an APPA-resistant threonine synthase homologue, which could serve as a self-

DOI: 10.1021/acschembio.9b00030
ACS Chem. Biol. XXXX, XXX, XXX−XXX

resistance mechanism to circumvent toxicity in the producing organism.

To assess this hypothesis, we reconstituted the activity of both the housekeeping *Bs*ThrC and the putative resistant RhiB *in vitro*. We demonstrate that RhiB is a PLP-dependent threonine synthase capable of generating threonine from PHSer. Kinetic assays revealed the enzyme to be 7-fold less efficient at generating threonine as compared to the *Bs*ThrC. However, while *Bs*ThrC is sensitive to APPA, RhiB was not subject to inhibition by this compound. We also determined the 2.0-Å resolution cocrystal structure of *Bs*ThrC in complex with APPA demonstrating that inhibition occurs via the formation of a covalent complex between APPA and the bound PLP cofactor. Structure-based analysis of the sensitive and resistant threonine synthases provide insights into the molecular basis for the observed APPA resistance in RhiB. This work uncovers the self-resistance mechanism utilized by *B. subtilis* ATCC 6633 against APPA, exemplifying one of many ways by which antibiotic producing bacteria can ensure self-resistance during the biosynthesis of a toxic metabolite.

RESULTS AND DISCUSSION

RhiB Is a Bona Fide Threonine Synthase Insensitive to APPA. For biochemical studies, recombinant RhiB was expressed and purified from an *E. coli* heterologous expression system, and its enzymatic activity was tested *in vitro*. Soluble His_6-RhiB required coexpression with the *E. coli* chaperones *GroEL/GroES*. Significantly, throughout the purification process, His_6-RhiB exhibited a yellow color characteristic of either a bound flavin or PLP cofactor. Threonine synthases characterized to date employ the use of PLP as a cofactor to convert *O*-phospho-L-homoserine into threonine.[5,17,18] UV−vis spectroscopy of purified His_6-RhiB revealed the presence of an absorption maximum at 420 nm characteristic of PLP-containing enzymes similar to other characterized threonine synthases (Supplementary Figure S1). We next sought to determine the ability of this enzyme to convert PHSer into threonine. Upon incubation of His_6-RhiB with PHSer, a new product appeared as observed by one-dimensional ^{1}H NMR with a doublet signal at 1.34 ppm and a *J* coupling constant of 6.4 Hz (Figure 2a). This diagnostic signal is characteristic of the H_γ present in threonine suggesting RhiB to be a threonine synthase.

In addition to RhiB, *B. subtilis* ATCC 6633 encodes for an endogenous ThrC (*Bs*ThrC) present within the threonine biosynthetic operon (Figure 1c). Recombinant *Bs*ThrC was purified as an N-terminal His_6 tagged construct, and the recombinant enzyme exhibited a UV−vis absorption maximum of 420 nm indicating this protein also copurified with PLP (Supplementary Figure S1). As with RhiB, enzyme activity assays with *Bs*ThrC incubated in the presence of PHSer led to the formation of threonine as observed by ^{1}H NMR (Figure 2b). Threonine formation was not detected in the absence of enzyme (Figure 2c,d).

To gain more insights into the efficiency of the enzymes in catalyzing the formation of threonine, steady state kinetic parameters for both enzymes were determined (Figure 3). Upon formation of threonine catalyzed by threonine synthases, inorganic phosphate is released as a product of the reaction.[19−21] Phosphate release was thus measured using a previously reported UV−vis continuous coupled spectrophotometric assay.[22] Recombinant *Bs*ThrC exhibited an apparent k_{cat} of 1.74 s^{-1} and an apparent K_M of 329 μM, while His_6-RhiB

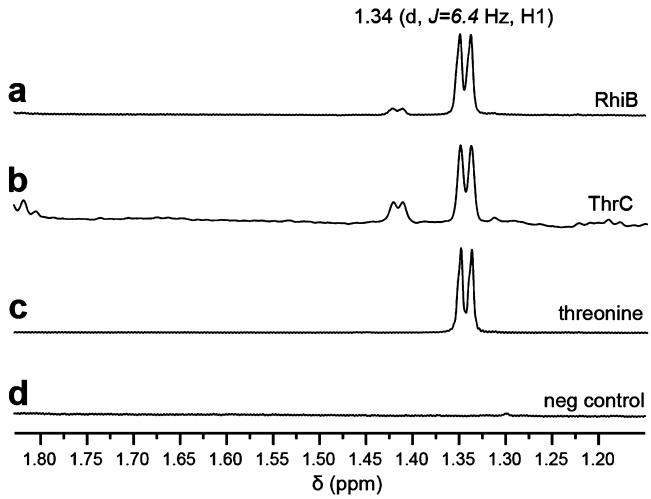

Figure 2. *In vitro* reconstitution of His_6-RhiB activity. ^{1}H NMR spectra of (a, b) reaction assays following incubation of PHSer with either (a) His_6-RhiB or (b) His_6-*Bs*ThrC, (c) threonine standard solution, and (d) reaction assay with no enzyme present. Only the upfield portion of the ^{1}H NMR spectrum is shown for clarity.

displayed an apparent k_{cat} of 0.60 s^{-1} and an apparent K_M of 824 μM.

The presence of two bona fide threonine synthases in *B. subtilis* ATCC 6633 suggests that RhiB might be an insensitive variant, which could serve as a self-resistance mechanism to avert APPA toxicity. To test this hypothesis, APPA was purified as previously described,[15] and the ability of RhiB and *Bs*ThrC to catalyze threonine formation was assessed in the presence of APPA by measuring PHSer consumption via ^{31}P NMR. Regardless of the APPA concentration used (either 5× or 20× molar excess), upon incubation of APPA with RhiB, no change in activity was observed compared to enzyme assays performed in the absence of APPA (Figure 4). Interestingly, incubation of *Bs*ThrC with APPA resulted in the formation of a new spectral feature at ∼519 nm (Supplementary Figure S2). This chromophore is consistent with the formation of a quinonoid species that may arise upon the enzymatic Cα proton abstraction from the APPA−PLP adduct.[2,3] This initial step is consistent with the enzymatic mechanism employed by threonine synthases, which commences with the abstraction of the alpha proton present in the PLP−PHSer adduct.[4] Activity assays performed with *Bs*ThrC in the presence of 5× molar excess APPA resulted in decreased enzymatic activity when compared to assays performed in the absence of APPA (Figure 4). These results suggest that APPA is capable of inhibiting *Bs*ThrC but not RhiB, proving that the latter is an APPA-insensitive threonine synthase.

Structural Characterization of *Bs*ThrC in Complex with APPA Reveals Mode of Inhibition. To establish the molecular basis by which APPA inhibits threonine synthase activity, we determined the 2.0-Å resolution X-ray crystal structures of *Bs*ThrC in its PLP and PLP−APPA bound states (Table 1). As expected, the overall structure of *Bs*ThrC is highly similar to other threonine synthases sharing the canonical fold-type II of PLP-dependent enzymes.[23,24] The overall fold of *Bs*ThrC recapitulates the architecture of other enzymes of the tryptophan synthase family.[23,24] The structure consists of an N-terminal α/β domain (domain 1; helices α1, α2, and α7−α11 and strands β1, β2, and β7−β10), followed by a second α/β domain (domain 2; helices α3−α6 and strands

DOI: 10.1021/acschembio.9b00030
ACS Chem. Biol. XXXX, XXX, XXX−XXX

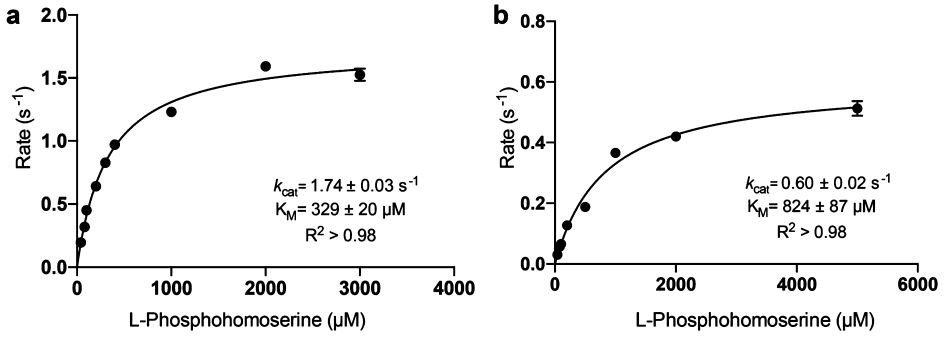

Figure 3. Kinetic characterization of His_6-RhiB and His_6-*Bs*ThrC. (a) His_6-*Bs*ThrC and (b) His_6-RhiB activity was measured by determining P_i release from *O*-phosphohomoserine. Enzymatic rates were plotted as a function of *O*-phosphohomoserine concentration, and the data were fit to the Michaelis−Menten equation. Results are means ± standard error of mean (SEM) of triplicate experiments.

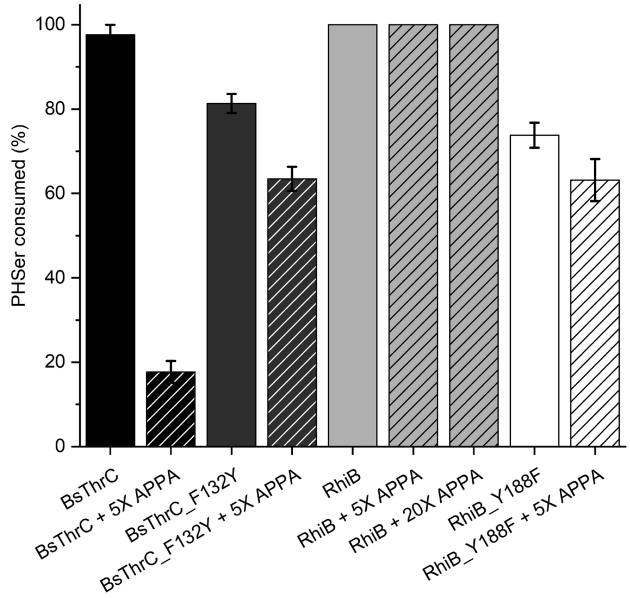

Figure 4. *Bs*ThrC and RhiB activity in the presence of APPA. End point assays were performed by measuring the amount of PHSer consumed at the end of the reaction. Data are plotted as the means ± standard error of the mean (SEM) of triplicate experiments. 5× APPA is 2.5 μM when incubated with *Bs*ThrC and 15 μM when incubated with RhiB. 20× APPA is 60 μM.

β3−β6) and a C-terminal tail (helices α12 and α13) that extends from one subunit to the other (Figure 5a). The enzyme active site forms at the interface of the two α/β domains of the same subunit while the C-terminal helix α13 interacts with domain 2 of the other subunit (Figure 5a,b).

Solution studies were consistent with a homodimeric assembly for *Bs*ThrC (Figure S1), and the two molecules in the crystallographic asymmetric unit of the enzyme recapitulated this functional homodimer (Figure 5a). In this homodimer, one subunit is in an open conformation with the PLP bound to the active site Lys59 through an aldimine linkage while the other subunit is in the closed conformation (Figure 5b−d). In the closed conformation, a ligand is bound to the cofactor even though no substrate was added during the purification or crystal screening process. However, the crystallization condition contained a mixture of amino acids (0.2 M sodium L-Glu, 0.2 M DL-Ala, 0.2 M Gly, 0.2 M DL-Lys HCl, 0.2 M DL-Ser). Modeling and refinement efforts support the judicious placement of Ala as the ligand adjacent to the PLP cofactor (Supplementary Figure S3). Consistent with this conclusion, prior experiments with *E. coli* threonine synthase show Ala as the substrate for half transamination reactions.[2] In

Table 1. Data Collection and Refinement Statistics

	*Bs*ThrC−PLP/ *Bs*ThrC−Ala (6CGQ)	*Bs*ThrC−APPA (6NMX)
Data Collection		
space group	$C222_1$	$P2_1$
a, *b*, *c* (Å), β (deg)	49.8, 127.9, 237.1	49.5, 104.2, 125.6, 99.6
resolution (Å)	118.5−2.0	123.8−1.97
R_{sym} (%)[a,b]	12.7 (102.7)	12.9 (85.2)
$I/\sigma(I)$	14.6 (2.2)	10.7 (2.1)
completeness (%)	100 (97.6)	91.3 (95.7)
redundancy	8.2 (8.4)	4.7 (4.7)
total reflns	411421	379109
unique reflns	50330	80926
Refinement		
resolution (Å)	49.7−2.0	123.8−1.97
no. reflns used	50265	80926
R_{work}/R_{free}[c]	0.18/0.23	0.16/0.21
Number of Atoms		
Protein	5121	10437
PO_4	5	
PLP	15	
PLP-Ala	21	
PLP−APPA		108
water	370	849
B-factors		
protein	28.23	22.93
PO_4	25.91	22.44
PLP	32.52	
PLP-Ala	21.08	
PLP−APPA		18.61
water	34.41	29.55
rms deviations		
bond lengths (Å)	0.007	0.007
bond angles (deg)	0.873	0.916
MOLPROBITY statistics		
clash score	2.71	4.13
Ramachandran outliers/ allowed/favored (%)	0.29/1.18/98.53	0.29/1.08/98.63

[a]Highest-resolution shell is shown in parentheses. [b]$R_{sym} = \sum|I_i - \langle I\rangle|/\sum I_i$, where I_i = intensity of the *i*th reflection and $\langle I\rangle$ = average intensity of symmetry-related observations of a unique reflection. [c]*R*-factor = $\sum|F_{obs} - F_{calc}|/\sum|F_{obs}|$ and *R*-free is the *R* value for a test set of reflections consisting of a random 5% of the diffraction data not used in refinement.

DOI: 10.1021/acschembio.9b00030
ACS Chem. Biol. XXXX, XXX, XXX−XXX

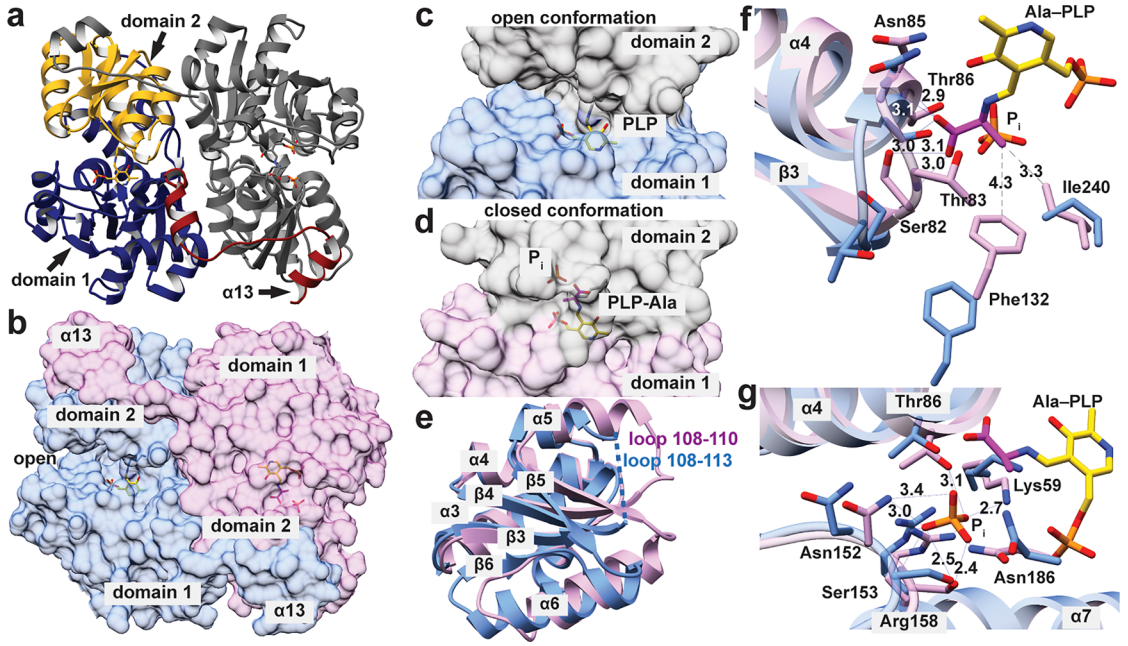

Figure 5. Crystal structure of *Bs*ThrC. (a) Ribbon diagram of the functional homodimer of *Bs*ThrC as generated by the space group symmetry operations. In blue is domain 1, in yellow is domain 2, and the C-terminal tail is shown in red. The helix α13 of one monomer interacts with the domain 2 of the other monomer. (b) Surface representation of the functional dimer. In blue is the *Bs*ThrC-PLP subunit in the open conformation and in pink is the *Bs*ThrC-Ala subunit in the closed conformation. (c, d) Zoomed in view of the surface in the open and closed conformations, respectively. Upon binding of the substrate, domain 2 (shown in gray) moves and closes the active site. Gray, domain 2, blue, domain 1 in the open state, pink, domain 1 in the closed state. (e) Conformational changes of domain 2 upon binding of the substrate. Only domain 2 is shown. Blue, open conformation, pink, closed conformation, dashed line, residues missing from crystal structure. (f, g) Stick representation of residues that interact with the bound ligands (alanine and phosphate, respectively) showing their position before (blue) and after (pink) binding. Dashed lines represent hydrophobic interactions and solid lines represent hydrogen bonding interactions (distances shown are in Å). Residues that interact with the cofactor are not shown.

addition, a phosphate group was also modeled in the active site of the *Bs*ThrC−Ala monomer (Supplementary Figure S3), which was presumably carried over during purification of the enzyme.

As observed in prior structures of threonine synthases, the enzyme undergoes a conformational change upon binding of the substrate (Ala) to control proton transfers and solvent accessibility during the reaction.[24−26] The superposition of the open and closed conformations reveals that major changes take place in domain 2 upon substrate binding (Figure 5d). Specifically, the loop that connects strand β4 with helix α5 (residues Gly108−Gly113) is disordered in the absence of substrate but becomes structured in the presence of substrate, with residues Phe112 and Gly113 adopting an α-helical conformation that extends helix α5. This change is accompanied by a significant movement of strands β3, β4, and β5 and helix α6 resulting in a closure of the active site. Finally, when the substrate binds, residues Asn152 and Ser153 are now within hydrogen bonding distance to the phosphate group of the substrate.

Crystals of *Bs*ThrC in complex with the inhibitor APPA showed an orange color, in agreement with the observed shift in the absorption spectrum of the enzyme after binding of the inhibitor (Supplementary Figure S2a,b and S4).[2] The complex crystallized as a dimer of functional dimers, and electron density corresponding to the inhibitor was present in all 4 molecules in the asymmetric unit (Figure 6a). Notably, the structure reveals that APPA binds to *Bs*ThrC by forming a covalent complex with the PLP cofactor and not with any of the residues in the active site (Figure 6a).

The structure of the *Bs*ThrC−APPA complex reveals a closed conformation, and a superposition with *Bs*ThrC bound to Ala shows that the active sites are nearly identical (Figure 6b). The carboxylate group of APPA is engaged by hydrogen bonding interactions with the hydroxyl group of the highly conserved Ser82 and the main chain amines of the highly conserved Thr83 and Thr86 (Figure 5f and Supplementary Figure S5). The inhibitor is further anchored by interactions between the phosphonate oxygens and the side chains of the highly conserved (among endogenous threonine synthases) Thr86, Asn152, Ser153, Arg158, and Asn186, as well as Lys59, which is the lysine that forms an aldimine linkage with PLP when the enzyme is in the resting state (Supplementary Figure S5). Finally, Phe132 and Ile240 line the enzyme pocket near the β, γ, and δ carbons of APPA further supporting the inhibitor (Supplementary Figure S5). Hence, APPA inhibits threonine synthase by mimicking the physiological substrate and trapping the enzyme in a closed conformation, and upon formation of the APPA−PLP adduct, ThrC abstracts the Cα proton from this species. This mechanism for inhibition is supported by the formation of a stable quinonoid intermediate (Supplementary Figure S2), and given the structural resemblance of APPA to PHSer, it is expected for the enzyme to be able to catalyze this initial step. When ThrC acts on the PLP derivative of PHSer, further proton abstractions on the adduct take place leading to the nonhydrolytic elimination of the phosphate in PHSer.[4,20,21,27] However, due to the presence of a stable C−P bond in APPA, the required nonhydrolytic elimination needed to yield threonine, hence resetting the catalytic cycle, is hampered preventing the enzyme from

DOI: 10.1021/acschembio.9b00030
ACS Chem. Biol. XXXX, XXX, XXX−XXX

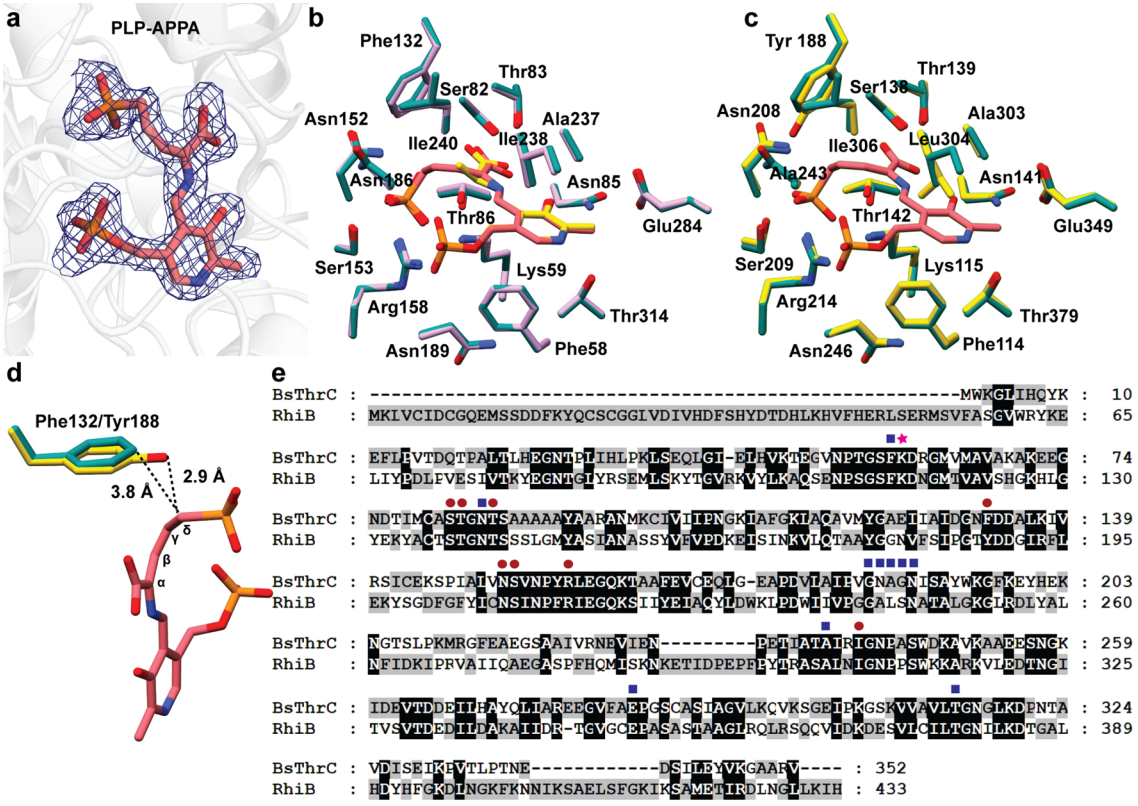

Figure 6. Crystal structure of *Bs*ThrC−APPA. (a) Difference Fourier map ($F_o - F_c$) calculated with the bound ligands removed prior to one round of refinement and map calculation and shown at a contour of 2.0σ (blue). It is evident from the electron density that the APPA is covalently bound to PLP and not to any active site residues. (b) Superposition of the *Bs*ThrC−APPA (teal) and *Bs*ThrC−Ala (pink) active sites. The two active sites are identical further supporting the hypothesis that APPA inhibits threonine synthase by "trapping" the enzyme in the closed conformation. The PLP−APPA adduct is shown in orange and the PLP−Ala adduct in yellow. (c) Superposition of *Bs*ThrC−APPA (teal) and RhiB (yellow) active sites. The RhiB model was generated by SWISS-MODEL[44] using the *Bs*ThrC−APPA structure as a template. The labels correspond to the RhiB residues. (d) Phe132 in *Bs*ThrC is ∼3.8 Å away from the Cδ of APPA. In RhiB, the corresponding Phe has been substituted by Tyr. (e) Sequence alignment of *Bs*ThrC and RhiB. Star, lysine that forms the internal aldimine; circles, residues that interact with APPA; squares, residues that interact with the cofactor.

completing a turnover thus trapping it in its "closed" state (Supplementary Figure S6). Due to the numerous proton abstractions and protonations occurring during the ThrC catalytic cycle, further spectroscopic studies of the PLP−APPA adduct following incubation with ThrC are warranted. Despite this limitation, our studies provide the first direct evidence for this previously proposed mechanism of ThrC inhibition by APPA.[2]

Structural Comparison of *Bs*ThrC and RhiB Active Sites Reveals Insights into the Structural Basis of RhiB Resistance to APPA. As no active site residues in *Bs*ThrC are involved in covalent interactions with the inhibitor, this raises the question as to why APPA is unable to inhibit RhiB. Presumably, APPA could bind to the PLP cofactor in RhiB as it does to *Bs*ThrC. To address this question, we generated a homology model for RhiB using the *Bs*ThrC−APPA structure as a template and compared their active sites. The most notable difference was the substitution of Phe132 in *Bs*ThrC with Tyr188 in RhiB (Figure 6c). In *Bs*ThrC, Phe132 is ∼3.8 Å away from the δ carbon of the phosphonic group of APPA, which is the position of the oxygen of the phosphate group in PHSer (Figure 6d). This led us to the hypothesis that introduction of a hydroxyl group in that position may affect binding of the inhibitor.

To investigate this hypothesis in detail, we generated the F132Y_*Bs*ThrC and Y188F_RhiB variants and performed activity assays in the absence and presence of APPA. The substitution of a Phe in Y188F_RhiB resulted in decreased enzymatic activity in the presence of 5× molar excess of APPA when compared to assays performed in the absence of inhibitor (Figure 4). Similarly, the substitution of a Tyr in F132Y_*Bs*ThrC resulted in a variant that was less sensitive to the inhibitor compared to the wild-type enzyme (Figure 4). These results suggest that the introduction of a hydroxyl group near the δ carbon of APPA affects its binding to PLP and the substitution of Phe132 in *Bs*ThrC with a Tyr188 in RhiB contributes to resistance to APPA in the latter enzyme. Interestingly, the activity levels seen in the Y188F_RhiB mutant suggest that while Tyr188 is important for rendering RhiB resistant to APPA additional structural features within RhiB must contribute as well for the observed APPA resistance.

A closer examination of the two active sites shows that the highly conserved Asn186 in *Bs*ThrC is substituted by Ala243 in RhiB (Figures 5g and 6b,c,e). As Asn186 is involved in engaging the phosphate group of the substrate PHSer (Figure 5g), the substitution of Asn186 and Phe132 in *Bs*ThrC by Ala243 and Tyr188 in RhiB may result in different binding orientation of the substrate−PLP adduct in RhiB, which may account for the 7-fold difference in the catalytic efficiencies (k_{cat}/K_M) of the two enzymes. As there is a complex network of interactions between the enzyme active site residues and the

DOI: 10.1021/acschembio.9b00030
ACS Chem. Biol. XXXX, XXX, XXX−XXX

different moieties of the cofactor−substrate/inhibitor adduct, it is very likely that in the RhiB active site the adduct is engaged in a shifted orientation. This presumed difference in binding orientation of the adduct may affect the binding kinetics or affinity of RhiB for APPA and is to be further investigated. Nonetheless, our mutagenesis data clearly show that the F132Y substitution in *Bs*ThrC is sufficient to render *Bs*ThrC less sensitive to the inhibitor.

CONCLUDING REMARKS

We show here that *Bacillus subtillis* ATCC 6633 possesses two threonine synthases, one that is sensitive (*Bs*ThrC) and one that is resistant (RhiB) to APPA, the active component of the rhizocticin natural product produced by this organism. In addition, our structural-sequence analyses between RhiB and the 2.0-Å resolution crystal structure of *Bs*ThrC in complex with APPA suggested that a single amino acid substitution in the RhiB active site (Tyr188) contributes to rendering this ThrC homologue resistant to APPA. In support of this finding, we generated a *Bs*ThrC variant tolerant to APPA by introducing a single site mutation within its active site (F132Y_*Bs*ThrC variant). Together, this work uncovers the self-resistance mechanism utilized by *B. subtilis* ATCC 6633 against APPA; the rhizocticin producing organism evades APPA toxicity by employing a second threonine synthase (RhiB) that is insensitive to APPA.

MATERIALS AND METHODS

BsThrC and RhiB Activity Assays. The following conditions were used to determine the ability of *Bs*ThrC and RhiB to catalyze threonine formation: 20 mM HEPES-NaOH, pH 7.5, 1 mM PHSer, 50 μM enzyme (either *Bs*ThrC or RhiB), and 5 μM PLP in a final volume of 500 μL, and samples were incubated for 2 h at 37 °C. Following the incubation period, proteins were removed using 3 kDa MWCO Amicon centrifugal filters (14 000*g*, 4 °C); the filtrate was collected and lyophilized to dryness. Dried solids were then dissolved in 500 μL of D_2O and analyzed via ^1H NMR.

Kinetic Characterization of BsThrC and RhiB. Michaelis−Menten kinetics were performed utilizing a coupled assay for the continuous monitoring of inorganic phosphate (P_i) release by the enzyme.[22] Briefly, in the presence of inorganic phosphate, 2-amino-6-mercapto-7-methylpurine riboside (MESG) is converted enzymatically by purine nucleoside phosphorylase (PNP) to ribose 1-phosphate and 2-amino-6-mercapto-7-methylpurine. This conversion of MESG results in a shift in maximum absorbance from 330 nm for the substrate to 360 nm for the product (ε_{360} = 11 000 M^{-1} cm^{-1}). This shift allows for continuous monitoring of P_i production by measuring the increase in absorbance at 360 nm. The following conditions were used: 50 mM HEPES-NaOH, pH 7.5, 100 μM PLP, 200 μM MESG, 0.00375 U μL^{-1} PNP, either 0.25 μM RhiB or 0.1 μM *Bs*ThrC, and various concentrations of *O*-phospho-L-homoserine (PHSer). Measurements were performed in triplicate.

Purification of Rhizocticin and APPA from *B. subtilis* 6633. Purification of rhizocticin was performed as previously described.[15] Following purification, acid hydrolysis with 6 M HCl was performed to obtain APPA following previously published procedures.[6,10]

Binding of APPA. Binding of the inhibitor to the enzyme was monitored spectrophotometrically by monitoring the formation of a chromophore at ∼500 nm.[2] *Bs*ThrC and RhiB were incubated with APPA (488 μM) in a 2:1 ratio for 15 min. Following the incubation period, both proteins were washed 5 times using 10 kDa MWCO Amicon centrifugal filters (500 μL, 14 000*g*, 4 °C, 20 min) with buffer (20 mM HEPES-NaOH, pH 7.5, 300 mM NaCl and 10% (v/v) glycerol), and the absorption spectra were recorded on a Cary 4000 UV−visible spectrophotometer at ambient temperature.

Crystallization of BsThrC. Initial crystallization conditions were determined by the sparse matrix sampling method using commercial screens. Crystals of *Bs*ThrC-APPA were grown using the hanging drop vapor diffusion method. Briefly, 1 μL of protein at 4 mg mL^{-1} concentration was incubated with 15 mol equiv of APPA (1.5 mM) for 1.5 h at ambient temperature, mixed with 1 μL of precipitant solution (0.03 M $MgCl_2$ hexahydrate, 0.03 M $CaCl_2$ dihydrate, 18% v/v PEG 550 MME, 9% w/v PEG 20000, 0.1 M MES/imidazole, pH 6.5), and equilibrated over a well containing the same precipitant solution at 9 °C. The crystals were sequentially soaked in precipitant solution supplemented with increasing concentrations of 20% (v/v) and 30% (v/v) ethylene glycol prior to vitrification by direct immersion in liquid nitrogen.

The *Bs*ThrC−Ala/*Bs*ThrC−PLP crystals were pooled from the initial screening trays. Briefly, 0.2 μL of protein at 6 mg mL^{-1} was mixed with 0.2 μL of MORPHEUS crystallization screen[28] condition H1 (0.2 M sodium L-glutamate, 0.2 M DL-alanine, 0.2 M glycine, 0.2 M DL-lysine HCl, 0.2 M DL-serine, 10% w/v PEG 20000, 20% v/v PEG MME 550, 0.1 M MES/imidazole, pH 6.5) using the sitting drop vapor diffusion method and equilibrated over a well containing the same precipitant solution at 9 °C. The crystals were sequentially soaked in precipitant solution supplemented with increasing concentrations of 20% (v/v) and 30% (v/v) ethylene glycol prior to vitrification by direct immersion in liquid nitrogen.

Data Collection, Phasing, and Structure Determination. X-ray diffraction data were collected at Life Sciences Collaborative Access Team (LS-CAT), Sector 21, Argonne National Laboratory. All data were indexed, integrated, and scaled using AutoProc.[29] Both structures were determined by molecular replacement as implemented in the Phenix program suite;[30] for the *Bs*ThrC−PLP/*Bs*ThrC−Ala structure, the coordinates of threonine synthase from *Aquifex aeolicus* Vf5 (59% sequence identity, 77% sequence similarity, 97% cover, PDB ID 2ZSJ) were used as a search model, while for the *Bs*ThrC−APPA complex the refined coordinates of *Bs*ThrC−PLP/*Bs*ThrC−Ala were used. In both cases, the resultant solutions were subsequently used as starting models for several rounds of automated model building using Phenix Autobuild[31] and Buccaneer,[32−34] followed by rounds of manual rebuilding using Coot,[35] and refinement using either Phenix Refine[36] or REFMAC5.[34] Ligands were built in Coot,[35] and the resultant models were further refined and manually inspected. In the final stages of refinement, water molecules were added with Phenix Refine and confirmed by manual inspection. In all cases, the quality of the in-progress model was routinely monitored using both the free *R* factor[37] and MolProbity[38] for quality assurance. The final models contain four Ramachandran outliers (Thr233 in chains A, B, and C and Thr337 in Chain D). These outliers are located on loops and were built to the best of our ability.

Inhibition Assays: ^{31}P NMR. Enzyme inhibition assays were carried out at 30 °C in 50 mM HEPES-NaOH (pH 7.5). In a final volume of 400 μL, 0.5 μM holo-*Bs*ThrC wild-type or mutant was preincubated with 2.5 μM APPA for 1 h at 30 °C, and then 1.6 mM PHSer (∼5 × K_M) was added. For RhiB wild-type and mutant, 3 μM holoenzyme was preincubated with 15 μM or 60 μM APPA for 1 h at 30 °C, and then 4 mM PHSer (∼5 × K_M) was added. After 30 min incubation of the enzymes with PHSer, the samples were passed through 10 kDa MWCO Amicon centrifugal filters, and 300 μL of the filtrate was removed and mixed with 300 μL of D_2O. For quantification during ^{31}P NMR, 0.5 mM dimethylphosphinic acid was added as internal standard in all samples, and PHSer consumption was measured for the calculation of enzyme activity. The activity of the enzymes in the presence of APPA was expressed as "percentage of PHSer consumed" with respect to the corresponding wild-type reaction that contained no APPA (considered as 100%). All measurements were performed in triplicate.

Estimation of PLP Content: Holoenzyme Concentration. Protein concentrations were determined by measuring the absorbance at 280 nm using the molecular weights and extinction coefficients calculated by the ProtParam tool (ExPASY server) (Table S3).[39] In order to calculate the concentration of holo-RhiB and holo-*Bs*ThrC in the protein preparations, the absorbance at 388 nm before (free PLP)

DOI: 10.1021/acschembio.9b00030
ACS Chem. Biol. XXXX, XXX, XXX−XXX

and after (total PLP) the addition of 0.2 M NaOH was measured, as previously described.[40−43] The difference between the two values corresponds to the PLP concentration that is bound to the enzyme (holoenzyme concentration). Free PLP has a maximum absorbance at 388 nm with an extinction coefficient of 6600 M^{-1} cm^{-1} in 0.1 M NaOH.[43] The ε_{388} of free PLP in 0.2 M NaOH was measured by using 40 μM and 80 μM PLP and was found to be ~6525 M^{-1} cm^{-1}. All measurements were performed in triplicate.

■ ASSOCIATED CONTENT

Supporting Information

The Supporting Information is available free of charge on the ACS Publications website at DOI: 10.1021/acschembio.9b00030.

Additional materials and methods, supporting figures, and supporting tables (PDF)

Accession Codes

The structures presented in this article have been deposited in the PDB under accession codes (6CGQ) and (6NMX).

■ AUTHOR INFORMATION

Corresponding Authors

*W.W.M. E-mail: metcalf@illinois.edu.

*S.K.N. E-mail: snair@illinois.edu.

ORCID

Satish K. Nair: 0000-0003-1790-1334

William W. Metcalf: 0000-0002-0182-0671

Author Contributions

⊥N.P. and M.A.O. contributed equally to this work.

Notes

The authors declare no competing financial interest.

■ ACKNOWLEDGMENTS

We thank the staff at Life Sciences Collaborative Access Team (LS-CAT, Argonne National Laboratory, Argonne, IL) for facilitating data collection. We also thank K.S. Ju, M.N. Goettge, E. Parkinson, M.M. López-Muñoz, and K.K. Wang for helpful discussions. Funded by NIH grants PO1GM077596 (to S.K.N. and W.W.M.) and R01GM127659 (to W.W.M.).

■ REFERENCES

(1) Metcalf, W. W., and van der Donk, W. A. (2009) Biosynthesis of Phosphonic and Phosphinic Acid Natural Products. *Annu. Rev. Biochem. 78*, 65−94.

(2) Laber, B., Gerbling, K. P., Harde, C., Neff, K. H., Nordhoff, E., and Pohlenz, H. D. (1994) Mechanisms of interaction of Escherichia coli threonine synthase with substrates and inhibitors. *Biochemistry 33*, 3413−3423.

(3) Laber, B., Lindell, S. D., and Pohlenz, H. D. (1994) Inactivation of Escherichia coli threonine synthase by DL-Z-2-amino-5-phospho-no-3-pentenoic acid. *Arch. Microbiol. 161*, 400−403.

(4) Flavin, M., and Slaughter, C. (1960) Threonine synthetase mechanism: studies with isotopic hydrogen. *J. Biol. Chem. 235*, 1112−1118.

(5) Skarstedt, M. T., and Greer, S. B. (1973) Threonine synthetase of Bacillus subtilis. The nature of an associated dehydratase activity. *J. Biol. Chem. 248*, 1032−1044.

(6) Rapp, C., Jung, G., Kugler, M., and Loeffler, W. (1988) Rhizocticins - new phosphono-oligopeptides with antifungal activity. *Liebigs Ann. Chem. 1988*, 655−661.

(7) Michener, H. D., and Snell, N. (1949) Two antifungal substances from Bacillus subtilis cultures. *Arch. Biochem. 22*, 208−214.

(8) Park, B. K., Hirota, A., and Sakai, H. (1976) Studies on new antimetabolite produced by microorganism. Part II. 2-Amino-5-phosphono-3-pentenoic acid, a new amino acid from N-1409 substance, an antagonist of threonine. *Agric. Biol. Chem. 40*, 1905−1906.

(9) Park, B. K., Hirota, A., and Sakai, H. (1977) Studies on new antimetabolite produced by microorganism. Part III. Structure of plumbemycin A and B, antagonists of L-threonine from Streptomyces plumbeus. *Agric. Biol. Chem. 41*, 573−579.

(10) Kugler, M., Loeffler, W., Rapp, C., Kern, A., and Jung, G. (1990) Rhizocticin A, an antifungal phosphono-oligopeptide of Bacillus subtilis ATCC 6633: biological properties. *Arch. Microbiol. 153*, 276−281.

(11) Capitani, G., Tschopp, M., Eliot, A. C., Kirsch, J. F., and Grutter, M. G. (2005) Structure of ACC synthase inactivated by the mechanism-based inhibitor L-vinylglycine. *FEBS Lett. 579*, 2458−2462.

(12) Amorim Franco, T. M., Favrot, L., Vergnolle, O., and Blanchard, J. S. (2017) Mechanism-Based Inhibition of the Mycobacterium tuberculosis Branched-Chain Aminotransferase by d- and l-Cycloserine. *ACS Chem. Biol. 12*, 1235−1244.

(13) Peisach, D., Chipman, D. M., Van Ophem, P. W., Manning, J. M., and Ringe, D. (1998) d-Cycloserine Inactivation of d-Amino Acid Aminotransferase Leads to a Stable Noncovalent Protein Complex with an Aromatic Cycloserine-PLP Derivative. *J. Am. Chem. Soc. 120*, 2268−2274.

(14) Jastrzebowska, K., and Gabriel, I. (2015) Inhibitors of amino acids biosynthesis as antifungal agents. *Amino Acids 47*, 227−249.

(15) Borisova, S. A., Circello, B. T., Zhang, J. K., van der Donk, W. A., and Metcalf, W. W. (2010) Biosynthesis of rhizocticins, antifungal phosphonate oligopeptides produced by Bacillus subtilis ATCC 6633. *Chem. Biol. 17*, 28−37.

(16) Schildkraut, I., and Greer, S. (1973) Threonine synthetase-catalyzed conversion of phosphohomoserine to alpha-ketobutyrate in Bacillus subtilis. *J. Bacteriol. 115*, 777−785.

(17) Flavin, M., and Slaughter, C. (1960) Purification and properties of threonine synthetase of Neurospora. *J. Biol. Chem. 235*, 1103−1108.

(18) Omi, R., Goto, M., Miyahara, I., Mizuguchi, H., Hayashi, H., Kagamiyama, H., and Hirotsu, K. (2003) Crystal structures of threonine synthase from Thermus thermophilus HB8: conformational change, substrate recognition, and mechanism. *J. Biol. Chem. 278*, 46035−46045.

(19) Murakawa, T., Machida, Y., and Hayashi, H. (2011) Product-assisted catalysis as the basis of the reaction specificity of threonine synthase. *J. Biol. Chem. 286*, 2774−2784.

(20) Shoji, M., Hanaoka, K., Ujiie, Y., Tanaka, W., Kondo, D., Umeda, H., Kamoshida, Y., Kayanuma, M., Kamiya, K., Shiraishi, K., Machida, Y., Murakawa, T., and Hayashi, H. (2014) A QM/MM study of the L-threonine formation reaction of threonine synthase: implications into the mechanism of the reaction specificity. *J. Am. Chem. Soc. 136*, 4525−4533.

(21) Ujiie, Y., Tanaka, W., Hanaoka, K., Harada, R., Kayanuma, M., Shoji, M., Murakawa, T., Ishida, T., Shigeta, Y., and Hayashi, H. (2017) Molecular Mechanism of the Reaction Specificity in Threonine Synthase: Importance of the Substrate Conformations. *J. Phys. Chem. B 121*, 5536−5543.

(22) Webb, M. R. (1992) A continuous spectrophotometric assay for inorganic phosphate and for measuring phosphate release kinetics in biological systems. *Proc. Natl. Acad. Sci. U. S. A. 89*, 4884−4887.

(23) Schneider, G., Kack, H., and Lindqvist, Y. (2000) The manifold of vitamin B6 dependent enzymes. *Structure 8*, R1−6.

(24) Eliot, A. C., and Kirsch, J. F. (2004) Pyridoxal phosphate enzymes: mechanistic, structural, and evolutionary considerations. *Annu. Rev. Biochem. 73*, 383−415.

(25) Wolfenden, R. (1974) Enzyme catalysis: conflicting requirements of substrate access and transition state affinity. *Mol. Cell. Biochem. 3*, 207−211.

(26) Schirch, V., Shostak, K., Zamora, M., and Guatam-Basak, M. (1991) The origin of reaction specificity in serine hydroxymethyltransferase. *J. Biol. Chem. 266*, 759−764.

DOI: 10.1021/acschembio.9b00030
ACS Chem. Biol. XXXX, XXX, XXX−XXX

(27) Garrido-Franco, M., Ehlert, S., Messerschmidt, A., Marinkovic, S., Huber, R., Laber, B., Bourenkov, G. P., and Clausen, T. (2002) Structure and function of threonine synthase from yeast. *J. Biol. Chem. 277*, 12396−12405.
(28) Gorrec, F. (2009) The MORPHEUS protein crystallization screen. *J. Appl. Crystallogr. 42*, 1035−1042.
(29) Vonrhein, C., Flensburg, C., Keller, P., Sharff, A., Smart, O., Paciorek, W., Womack, T., and Bricogne, G. (2011) Data processing and analysis with the autoPROC toolbox. *Acta Crystallogr., Sect. D: Biol. Crystallogr. 67*, 293−302.
(30) Adams, P. D., Afonine, P. V., Bunkoczi, G., Chen, V. B., Davis, I. W., Echols, N., Headd, J. J., Hung, L.-W., Kapral, G. J., Grosse-Kunstleve, R. W., McCoy, A. J., Moriarty, N. W., Oeffner, R., Read, R. J., Richardson, D. C., Richardson, J. S., Terwilliger, T. C., and Zwart, P. H. (2010) PHENIX: a comprehensive Python-based system for macromolecular structure solution. *Acta Crystallogr., Sect. D: Biol. Crystallogr. 66*, 213−221.
(31) Terwilliger, T. C., Grosse-Kunstleve, R. W., Afonine, P. V., Moriarty, N. W., Zwart, P. H., Hung, L. W., Read, R. J., and Adams, P. D. (2008) Iterative model building, structure refinement and density modification with the PHENIX AutoBuild wizard. *Acta Crystallogr., Sect. D: Biol. Crystallogr. 64*, 61−69.
(32) Cowtan, K. (2006) The Buccaneer software for automated model building. 1. Tracing protein chains. *Acta Crystallogr., Sect. D: Biol. Crystallogr. 62*, 1002−1011.
(33) Cowtan, K. (2008) Fitting molecular fragments into electron density. *Acta Crystallogr., Sect. D: Biol. Crystallogr. 64*, 83−89.
(34) Winn, M. D., Ballard, C. C., Cowtan, K. D., Dodson, E. J., Emsley, P., Evans, P. R., Keegan, R. M., Krissinel, E. B., Leslie, A. G., McCoy, A., McNicholas, S. J., Murshudov, G. N., Pannu, N. S., Potterton, E. A., Powell, H. R., Read, R. J., Vagin, A., and Wilson, K. S. (2011) Overview of the CCP4 suite and current developments. *Acta Crystallogr., Sect. D: Biol. Crystallogr. 67*, 235−242.
(35) Emsley, P., Lohkamp, B., Scott, W. G., and Cowtan, K. (2010) Features and development of Coot. *Acta Crystallogr., Sect. D: Biol. Crystallogr. 66*, 486−501.
(36) Afonine, P. V., Grosse-Kunstleve, R. W., Echols, N., Headd, J. J., Moriarty, N. W., Mustyakimov, M., Terwilliger, T. C., Urzhumtsev, A., Zwart, P. H., and Adams, P. D. (2012) Towards automated crystallographic structure refinement with phenix.refine. *Acta Crystallogr., Sect. D: Biol. Crystallogr. 68*, 352−367.
(37) Read, R. J., Adams, P. D., Arendall, W. B., 3rd, Brunger, A. T., Emsley, P., Joosten, R. P., Kleywegt, G. J., Krissinel, E. B., Lutteke, T., Otwinowski, Z., Perrakis, A., Richardson, J. S., Sheffler, W. H., Smith, J. L., Tickle, I. J., Vriend, G., and Zwart, P. H. (2011) A new generation of crystallographic validation tools for the protein data bank. *Structure 19*, 1395−1412.
(38) Chen, V. B., Arendall, W. B., Headd, J. J., Keedy, D. A., Immormino, R. M., Kapral, G. J., Murray, L. W., Richardson, J. S., and Richardson, D. C. (2010) MolProbity: all-atom structure validation for macromolecular crystallography. *Acta Crystallogr., Sect. D: Biol. Crystallogr. 66*, 12−21.
(39) Wilkins, M. R., Gasteiger, E., Bairoch, A., Sanchez, J. C., Williams, K. L., Appel, R. D., and Hochstrasser, D. F. (1998) Protein identification and analysis tools in the ExPASy server. *Methods Mol. Biol. 112*, 531−552.
(40) Kulikova, V. V., Zakomirdina, L. N., Bazhulina, N. P., Dementieva, I. S., Faleev, N. G., Gollnick, P. D., and Demidkina, T. V. (2003) Role of Arginine 226 in the Mechanism of Tryptophan Indole-Lyase from Proteus vulgaris. *Biochemistry (Moscow) 68*, 1181−1188.
(41) Pennacchietti, E., Lammens, T. M., Capitani, G., Franssen, M. C., John, R. A., Bossa, F., and De Biase, D. (2009) Mutation of His465 alters the pH-dependent spectroscopic properties of Escherichia coli glutamate decarboxylase and broadens the range of its activity toward more alkaline pH. *J. Biol. Chem. 284*, 31587−31596.
(42) Tramonti, A., John, R. A., Bossa, F., and De Biase, D. (2002) Contribution of Lys276 to the conformational flexibility of the active site of glutamate decarboxylase from Escherichia coli. *Eur. J. Biochem. 269*, 4913−4920.
(43) Peterson, E. A., and Sober, H. A. (1954) Preparation of Crystalline Phosphorylated Derivatives of Vitamin B6. *J. Am. Chem. Soc. 76*, 169−175.
(44) Bordoli, L., Kiefer, F., Arnold, K., Benkert, P., Battey, J., and Schwede, T. (2009) Protein structure homology modeling using SWISS-MODEL workspace. *Nat. Protoc. 4*, 1.

DOI: 10.1021/acschembio.9b00030
ACS Chem. Biol. XXXX, XXX, XXX−XXX